

1 ***In situ* Raman spectroscopic evidence for oxygen reduction**
2 **reaction intermediates at platinum single crystal surfaces**

3 Jin-Chao Dong¹, Xia-Guang Zhang¹, Valentín Briega-Martos², Xi Jin¹, Ji Yang¹, Shu Chen³,
4 Zhi-Lin Yang³, De-Yin Wu¹, Juan Miguel Feliu^{2,*}, Christopher T. Williams⁴, Zhong-Qun
5 Tian¹, Jian-Feng Li^{1,3,5,*}

6 ¹MOE Key Laboratory of Spectrochemical Analysis and Instrumentation, State Key Laboratory of
7 Physical Chemistry of Solid Surfaces, iChEM, and College of Chemistry and Chemical
8 Engineering, Xiamen University, Xiamen 361005, China

9 ²Instituto de Electroquímica, Universidad de Alicante, Apt. 99, Alicante, E-03080, Spain

10 ³Department of Physics, Research Institute for Biomimetics and Soft Matter, Xiamen University,
11 Xiamen 361005, China

12 ⁴Department of Chemical Engineering, University of South Carolina, Columbia, South Carolina
13 29208, USA

14 ⁵Shenzhen Research Institute of Xiamen University, Shenzhen 518000, China

15 Email: Li@xmu.edu.cn and juan.feliu@ua.es

16

17 **Abstract**

18 Developing an understanding of structure-activity relationships and reaction mechanisms of
19 catalytic processes is critical to the successful design of highly efficient catalysts. As a

1 fundamental reaction in fuel cells, elucidation of the oxygen reduction reaction (ORR) mechanism
2 at Pt(*hkl*) surfaces has remained a significant challenge for researchers. Here, we employ *in situ*
3 electrochemical surface-enhanced Raman spectroscopy (SERS) and density functional theory
4 (DFT) calculation techniques to examine the ORR process at Pt(*hkl*) surfaces. Direct
5 spectroscopic evidences for ORR intermediates indicates that under acid conditions, the pathway
6 of ORR at Pt(111) occurs through the formation of HO₂*, while at Pt(110) and Pt(100) it occurs
7 via the generation of OH*. However, we propose that the pathway of ORR under alkaline
8 conditions at Pt(*hkl*) surfaces mainly occurs through the formation of O₂⁻. Significantly, these
9 results demonstrate that the SERS technique offers an effective and reliable way for real-time
10 investigation of catalytic processes at atomically flat surfaces.

11

12 In recent energy researches, significant focus has been placed on understanding the mechanism of
13 catalytic reactions at the atomic level. The direct operando monitoring of surface catalytic
14 reactions has always been a "holy grail" in electrochemistry and heterogeneous catalysis, and will
15 aid significantly in the design and development of more highly efficient catalysts.^{1,2} As a classical
16 catalytic reaction, the process and mechanism of the oxygen reduction reaction (ORR) at platinum
17 surfaces have been a focus of attention in the literature for a long time.^{3,4} Though lots of research
18 groups have carried out experimental and theoretical studies to reveal the ORR mechanism, the
19 detailed surface process is still not clear.

20 Generally, the mechanism of ORR process at platinum electrodes in acidic condition is
21 considered to occur by two main pathways: one involves oxygen being reduced directly via a

1 four-electron pathway into H₂O; the other first reacts oxygen via a two-electron pathway to
2 hydrogen peroxide, followed by a two electron transfer reduction of the latter to water; hydrogen
3 peroxide also can directly diffuse into the solution as a final product, which then quickly
4 decomposes. However, some essential questions and uncertainties remain about ORR processes,
5 including slow kinetics, the origin of observed high overpotentials, and the rate determining
6 step.⁵⁻¹¹ The main reason is that as a multi-electron reaction, there are varieties of intermediates
7 (e.g., OH*, O₂²⁻, O₂⁻, HO₂*, etc.) that are generated during ORR process, and most of the
8 intermediates have a short life-time, low coverage and are also influenced by other co-adsorbed
9 species. Thus, the key factor to unravel the ORR mechanism is to develop an *in situ* method to
10 identify the various reaction intermediates and their adsorbed configurations at platinum surfaces
11 during the ORR process. With their well-defined surface structures, optical and electric field
12 properties, and ability to be modeled at the atomic level, single crystal surfaces play a key role in
13 probing catalytic reaction mechanisms in surface science.¹² However, most of the current
14 spectroscopic methods are not suitable for the single crystal studies in aqueous solution, especially
15 for the ORR reaction at Pt(*hkl*) electrode surfaces.¹³⁻¹⁹

16 Surface-enhanced Raman scattering (SERS) is a powerful fingerprint spectroscopy that can be
17 used for *in situ* investigation of trace chemical species and identification with single-molecule
18 sensitivity.²⁰⁻²² However, its applications are generally restricted to ‘free-electron-like’ metals such
19 as Au, Ag and Cu that have non-smooth surfaces. To overcome the long-term limitation of SERS
20 on morphology and material generality, previously we developed a surface vibrational
21 spectroscopic method that was named Shell-Isolated Nanoparticle-Enhanced Raman Spectroscopy
22 (SHINERS).²³ In SHINERS, an ultrathin and uniform silica shell coated onto a gold nanoparticle

1 can efficiently enhance the Raman signal of molecules that are in located near the nanoparticle
2 surface without any interference. It is possible to obtain Raman signals from any substrate and any
3 material surface. A unique advantage of SHINERS is its particular applicability to explore the
4 adsorption configuration and catalytic processes of probe molecules at single crystal surfaces.²⁴⁻³²

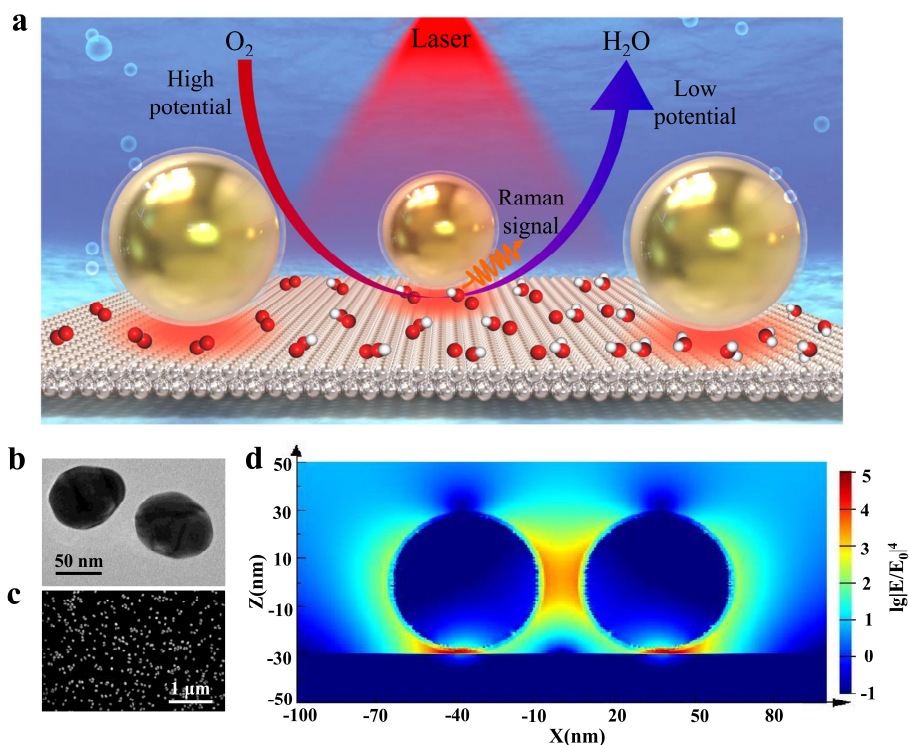
5 Here, we employ *in situ* electrochemical (EC)-SHINERS coupled with density functional theory
6 (DFT) calculations to study the ORR process at Pt(*hkl*) electrode surfaces. We obtain direct
7 spectral evidence that allows the ORR mechanism at these surfaces to be elucidated at a molecular
8 and atomic level.

9

10 **SHINERS enhancement at Pt(*hkl*) surfaces**

11 For a clear understanding of the relationship between the shell-isolated nanoparticles (SHINs)
12 enhancement and the electric field distribution, a 2×2 Au@SiO₂ nanoparticles (NPs) array was
13 modeled on a perfectly smooth platinum substrate surface and simulated using a
14 3D-Finite-Difference Time-Domain (3D-FDTD) theoretical system. Fig. 1a shows the schematic
15 diagram of *in situ* EC-SHINERS at low index Pt(*hkl*) surfaces. The SHINs used in this experiment
16 had a gold nanoparticle core (~55 nm) with SiO₂ shell (~2 nm) (Fig. 1b and Supplementary Fig. 1),
17 with the coverage of SHINs at the Pt(*hkl*) electrode surface at around 30% (Fig. 1c). The
18 3D-FDTD technique has been employed to model the SHINERS system effectively.³³⁻³⁶ The hot
19 spots are mainly located around the particle-surface junctions under 638 nm excitation (Fig. 1d),
20 and the average SERS enhancement factor of this configuration is about 1.0×10^5 on the Pt(*hkl*)
21 surface.²⁴

1



2

3 **Figure 1 | Schematic illustration of SHINERS study of ORR process and correlated characterization and**

4 **3D-FDTD results at Pt(*hkl*) surface. (a) The model of shell-isolated nanoparticles (Au@SiO₂ NPs, SHINs) at**

5 **Pt(111) surface, and the mechanism of ORR process revealed by EC-SHINERS method. The silver-white, red, and**

6 **white spheres represent Pt, O, and H atoms, respectively. The large golden spheres with transparent shells**

7 **represent SHINs. The SHINs, when being excited by a laser, can generate strong electromagnetic fields to enhance**

8 **the Raman signals of molecules adsorbed at the Pt(*hkl*) single crystal surface. (b) The transmission electron**

9 **microscope (TEM) image of Au@SiO₂ nanoparticle. (c) Scanning electron microscope (SEM) image of Pt(111)**

10 **single crystal electrode surface modified with SHINs. (d) 3D-FDTD simulations of four SHINs NPs with a model**

11 **of 2 × 2 array on a Pt substrate.**

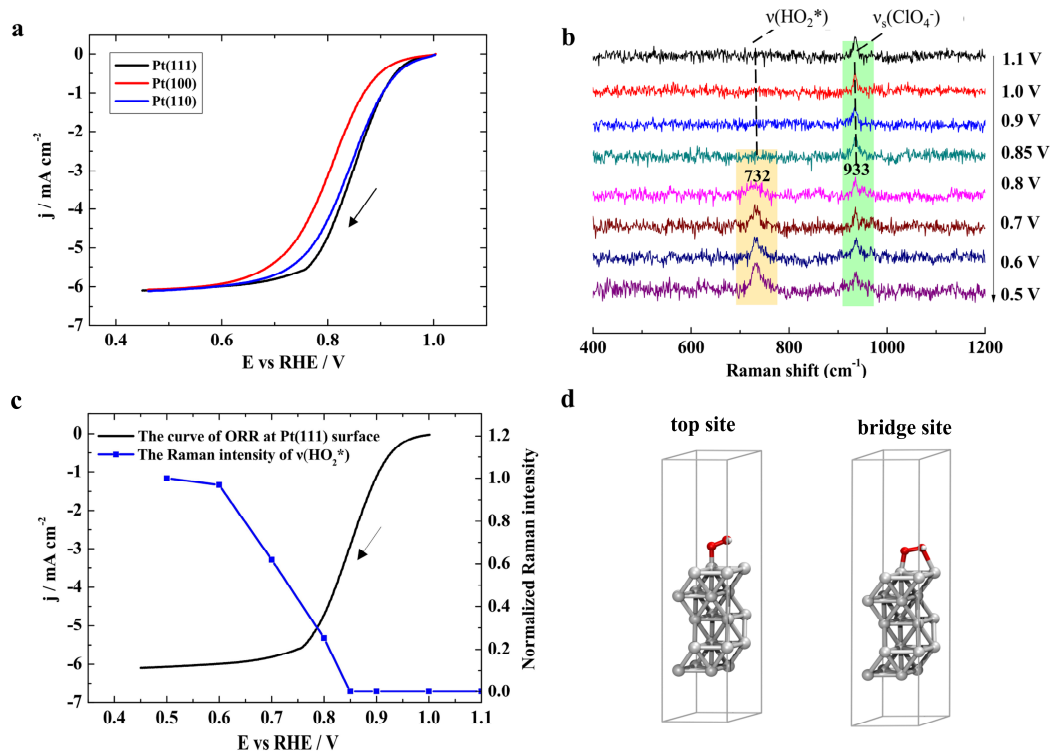
12

13 **ORR processes at Pt(*hkl*) surfaces in acidic condition**

14 **First, we obtained the polarization curves of ORR process at three Pt(*hkl*) rotating disk electrode**

1 surfaces in 0.1 M HClO₄ electrolyte solution saturated with O₂ respectively; the rotation rate was
2 1600 rpm. We can find that the ORR activity of Pt(*hkl*) decreased in the sequence (111) > (110) >
3 (100) in HClO₄ solution (Fig. 2a). The O₂ reduction current begins around 1.0 V and then quickly
4 achieves its limiting diffusion current around 0.7 V following the negative swept direction (Fig. 2a
5 and Supplementary Fig. 5). In limiting diffusion potential range (0.3 V ~ 0.7 V), the ORR activity
6 of Pt(*hkl*) is completely controlled by the mass transfer of oxygen. When potential decreases
7 below 0.3 V, the limiting diffusion current begins to decrease due to hydrogen adsorption at Pt(*hkl*)
8 electrode surface. The adsorbed hydrogen increases the difficulty of breaking the O-O bond of
9 oxygen molecules, as there are not enough adjacent vacancies for O₂ adsorption at Pt(*hkl*) surfaces.
10 As a result, the oxygen molecules will partly form H₂O₂.³⁷ As can be observed in Fig. 2a, the onset
11 potential of ORR for Pt(111) and Pt(110) is similar, while it is much lower for Pt(100). In previous
12 works it was observed that the activity for the ORR increases as the number of (110) steps
13 increases in stepped surfaces with (111) terraces, the activity for the ORR increases, being Pt(110)
14 therefore more active than Pt(111).³⁸ In this work this difference is less noticeable since the
15 negative-going sweeps from 1.0 V are shown (in order to compare them with the spectroscopic
16 results), and Pt(110) initially presents PtO species (Supplementary Note 1 and Supplementary Fig.
17 2). Therefore, in the negative-going sweeps the activity of Pt(110) is partially inhibited by the
18 presence of this surface oxides. In the positive-going scans the surface oxides are not present,
19 recovering then the previously reported activity. To explore the ORR mechanism at Pt(*hkl*)
20 surfaces, *in situ* EC-SHINERS method was employed to evaluate the ORR system in the 0.1 M
21 HClO₄ solution. Since the electrode in the Raman cell is not able to rotate during the ORR
22 experiment, the limiting ORR diffusion current is somewhat different when compared to the

1 rotating disk electrode (RDE) system. Nevertheless, the starting potential and the potential range
 2 of ORR without rotation were almost the same as the RDE system (Supplementary Note 4 and
 3 Supplementary Fig. 5-6).



4
 5 **Figure 2 | The electrochemical results of ORR process at Pt(*hkl*) surfaces in acidic condition, and correlated**
 6 **EC-SHINERS and DFT results of ORR at Pt(111) surface. (a)** The polarization curves of ORR process at three
 7 Pt(*hkl*) rotating disk electrodes in oxygen saturated 0.1 M HClO₄ solutions, the rotation rate was 1600 rpm, and the
 8 scan rate was 50 mV/s; **(b)** EC-SHINERS spectra of ORR system at Pt(111) electrode surface in 0.1 M HClO₄
 9 solution saturated with O₂; **(c)** Normalized EC-SHINERS intensities of stretching mode of O-OH around 732 cm⁻¹
 10 at different potentials. The polarization curve of ORR process at Pt(111) surface in 0.1 M HClO₄ solution saturated
 11 with O₂, the rotation rate was 1600 rpm, the scan rate was 50 mV/s. The arrows in panel a, b, and c represent the
 12 potential scanning direction, and all the potentials are relative to RHE; **(d)** Side-view illustrations of HO₂* at

1 different stable adsorption configurations at Pt(111) surface on top site and bridge site adsorption structures. The
2 silver-gray, red, and white spheres represent Pt, O, and H atoms, respectively.

3

4 The EC-SHINERS spectra of ORR at Pt(111) electrodes were obtained over the potential range
5 from 1.1 V to 0.5 V. During the negative potential excursion, there was no observable Raman
6 signal in the range of 400 to 1200 cm^{-1} until 0.8 V except the peak at 933 cm^{-1} (Fig. 2b). The peak
7 at 933 cm^{-1} was attributed to the symmetric stretch mode of the perchlorate ion, $\nu_s(\text{ClO}_4^-)$. As the
8 potential decreased, another obvious Raman band around 732 cm^{-1} in the acidic solution appeared
9 when the potential arrived 0.8 V, which upon further increase to 0.6 V (Fig. 2c). Furthermore, a
10 deuterium isotopic substitution measurement was carried out (Supplementary Note 5 and
11 Supplementary Fig. 7). In deuterium isotopic experiment, the peaks around 732 cm^{-1} were shifted
12 to lower wavenumber around 705 cm^{-1} , which implied that the intermediates should be correlated
13 with an “H” atom. While the first candidate considered of 732 cm^{-1} involves the O-O stretching
14 vibration of H_2O_2 , this molecule is unlikely to be stable at the Pt(111) surface, and would be
15 immediately oxidized or reduced further to oxygen or water. According to electrochemical
16 results,^{39,40} we can confirm that the peak around 732 cm^{-1} belongs to O-O stretching vibration of
17 adsorbed HO_2^* on Pt(111), which also can be considered as an important intermediate species of
18 ORR process.⁴⁰ DFT method was also employed to calculate the vibrational frequencies of HO_2^*
19 species at Pt(111) (Supplementary Note 12 and Supplementary Fig. 21). From the DFT results, we
20 found that there were two different stable adsorption configurations of HO_2^* at the Pt(111) surface,
21 on top (t-b) site and bridge (b-b) site (Fig. 2d) (the distance of Pt-O were 2.008 Å and 2.020 Å,
22 respectively) adsorption structures, and the correlated Raman frequency of O-O stretching

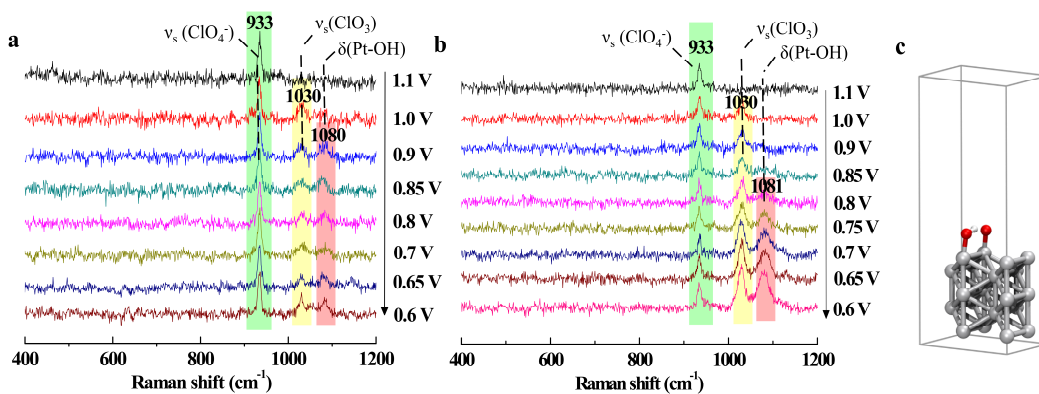
1 vibration for these two different structures were 839 cm^{-1} and 726 cm^{-1} respectively. This means
2 that the peaks around 732 cm^{-1} in our experiment can be assigned to the O-O stretching vibration
3 of b-b adsorption structure of HO_2^* .

4 In general, for the ORR process at the Pt(111) surface in an acidic solution, at high potentials,
5 the oxygen reduces to water through the particular intermediates, and at low potentials the oxygen
6 reduction to water was inhibited and stops at the peroxide stage (perhaps involving the same
7 intermediates). To further understand the ORR mechanism at Pt(111) surface in acidic conditions,
8 we tried to look at the ORR process from higher to lower potentials range compared the range of
9 1.1 V to 0.5 V at Pt(111) (Supplementary Note 6 and Supplementary Fig. 8a). At 1.2 V potential,
10 there was an obvious Raman peak at around 571 cm^{-1} and its frequency shifted to lower
11 wavenumber until at 0.9 V it was 567 cm^{-1} . This peak was attributed to the Pt-O stretching mode.⁴¹
12 Meanwhile, the peak of HO_2^* at 732 cm^{-1} was observed when the potential arrived 0.75 V and its
13 intensity increased until 0.6 V, after which is remained stable following further a potential
14 decrease. Finally, the 732 cm^{-1} peak intensity decreased when the potential was below to 0.4 V,
15 which correlated well with the ORR current results (Supplementary Fig. 8b).

16 According to electrochemical researches, Pt(111) is saturated with about 1/3 monolayer of OH
17 at 0.8 V and will then decrease to zero at the upper end of the double layer region.^{42,43} However,
18 we did not find the OH species at $\sim 0.8\text{ V}$ during the ORR process at Pt(111) surface by SHINERS.
19 Recent work shows that the O-H bond being nearly parallel with the Pt(111) surface at 0.8 V,⁴⁴
20 while the SHINERS method requires a vibrational dipole component normal to the surface in
21 order to undergo light absorption. This special structure of OH at Pt(111) surface may be the
22 reason why we do not detect the OH adsorption at Pt(111) by SHINERS around 0.8 V. For the

1 ORR process, in the kinetic potential region, there will be a low concentration of available sites
2 for forming adsorbed HO_2^* , rendering the signal too weak to be observed. Following the potential
3 sweeps in the negative direction, the coverage of OH drops rapidly, opening up more sites for O_2
4 to approach and form adsorbed HO_2^* . Thus, the SHINERS spectra clearly show the formation of
5 adsorbed HO_2^* at 0.8 V. Reaching about 0.6 V, there is no longer adsorbed OH and the potential
6 continues through the double layer region until somewhat less than 0.4 V, when underpotential
7 deposited (UPD) H starts to block sites. The potential dependence of the current density, in
8 Supplementary Fig. 8, illustrates that shortly after entering the diffusion-limited region and double
9 layer region, there is surface congestion with adsorbed HO_2^* intermediates.

10 In addition, we have carefully compared the electrochemical behaviors with and without SHINs
11 on Pt(111), Pt(100), and Pt(110) single crystal surfaces during the ORR process (Supplementary
12 Notes 2-3, Supplementary Fig. 3-4 and Supplementary Fig. 9). From the experimental results, we
13 find that the SHINs only affect the spectroscopy, but not the activity of Pt(*hkl*) surfaces for ORR
14 reaction. From theoretical and experiment results, we can assure that SHINERS method can
15 identify different adsorption structure of surface adsorbate species. Combining with the
16 electrochemical result,³⁹ we assert that the HO_2^* species is an important intermediate of the ORR
17 process under acidic conditions. Moreover, we will further discuss about the ORR mechanism at
18 the Pt(*hkl*) surface in the section of “Mechanism of ORR process at Pt(*hkl*) surfaces”.



1

2 **Figure 3 | *In situ* EC-SHINERS results of ORR at Pt(100) and Pt(110) surfaces in acidic condition and DFT**

3 **result of OH* at Pt(110) surface. (a) EC-SHINERS spectra of ORR at a Pt(100) electrode surface in 0.1 M**

4 **HClO₄ solution; (b) EC-SHINERS spectra of ORR at a Pt(110) electrode surface in 0.1 M HClO₄ solution. The**

5 **arrows in panel a and b represent the potential scanning direction, and all the potentials are relative to RHE; (c)**

6 **Side-view illustrations of OH* and O* at a Pt(110) surface. The silver-gray, red, and white spheres represent Pt, O,**

7 **and H atoms, respectively.**

8

9 The crystallographic orientation and the surface structure of the single crystal electrode surface

10 will greatly influence the reaction mechanism and reaction kinetics. Moreover, the ORR activity is

11 also highly sensitive to the surface structure of the Pt(*hkl*) electrode. We therefore investigated the

12 ORR processes at the other two low-index Pt(*hkl*) surfaces (i.e., Pt(110) and Pt(100)) in 0.1 M

13 HClO₄ solution saturated with O₂. Interestingly, we observed different phenomenon at the three

14 low-index Pt(*hkl*) surfaces from SHINERS experimental results. There were two Raman peaks,

15 around 1030 cm⁻¹ and 1080 cm⁻¹, that appeared at Pt(100) following a decrease in potential, and

16 the phenomenon at Pt(110) surface was similar with Pt(100) (Fig. 3), but their relative Raman

17 intensity and onset potential were different. At the same time, the deuterium isotopic substitution

18 measurement was taken into consideration as before (Supplementary Note 7 and Supplementary

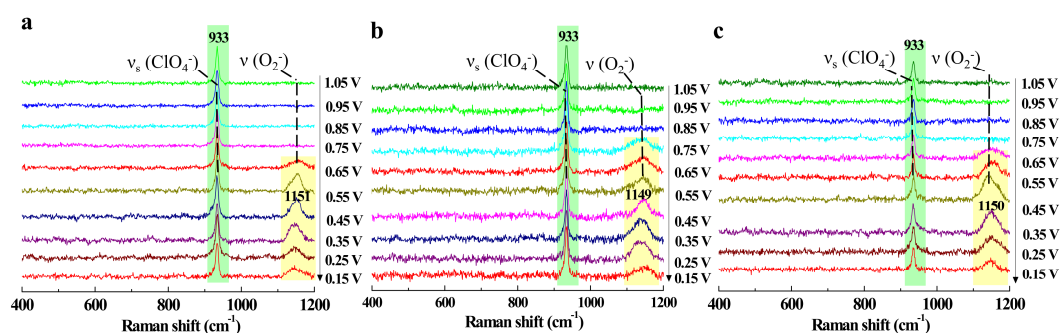
1 Fig. 10). We did not observe any obvious shift in the 1030 cm^{-1} feature, but the peak at 1080 cm^{-1}
2 shifted to a lower wavenumber around $\sim 717\text{ cm}^{-1}$ during the D_2O experiment. Meanwhile, in the
3 $^{18}\text{-O}_2$ isotopic substitution experiment at Pt(110) surface (Supplementary Note 8 and
4 Supplementary Fig. 11), we found that the peak around 1030 cm^{-1} did not show any obvious shift,
5 while the peak around 1080 cm^{-1} was shifted to a lower wavenumber around 1072 cm^{-1} , which
6 further implied that the intermediates of 1080 cm^{-1} correlated with oxygen related species.
7 According to the literature,^{14,45} the peak around 1030 cm^{-1} can be assigned to the symmetric
8 stretching vibrational mode of ClO_3 in HClO_4 molecule, and the band around 1080 cm^{-1} can be
9 assigned to the platinum-hydroxide bending mode δ_{PtOH} of OH^* (Fig. 3c).

10 The DFT calculated results showed that if only OH^* adsorbed at the Pt(110) surface,
11 (Supplementary Note 13 and Supplementary Fig. 22) the Pt-OH bending would appear at 875 cm^{-1} .
12 But if OH^* adsorbed at an atop site with an atomic oxygen on the nearest neighbor, the adsorbed
13 O^* atom plays a constructive role in bending the H atom (Fig.3c). In this case, the Pt-OH bending
14 vibration increases to 1078 cm^{-1} , which correlates well with the experimental and reference results.
15 From DFT calculation results, we also found that the HO_2^* species were not so stable at Pt(110)
16 and Pt(100) surfaces, being easily dissociated to Pt-O and Pt-OH because of the lower
17 coordination number of Pt in Pt(110) and Pt(100). On the other hand, the different ORR activity of
18 Pt(100) and Pt(110) compared to Pt(111) maybe due to presence of OH^* on the surfaces, which
19 can block the active site of platinum surfaces.

20

21 **ORR processes at Pt(*hkl*) surfaces in alkaline condition**

1 Under electrochemical conditions, the interfacial state of Pt(*hkl*) electrode surface should undergo
 2 some changes following the pH value increase. For example, the charge distribution and the
 3 adsorption state at the interface will change significantly. Since the ORR process is a typical
 4 electrode reaction to consume protons and generate OH*, the interface pH values will be changed
 5 as the reaction proceeds. During this process, the ORR reaction pathway, intermediates and their
 6 surface coverage rate at the electrode surface will be changed. Therefore, it is necessary to study
 7 the ORR mechanism at different pH values, which will give us more important information about
 8 the relationship between the interface structures and the reaction mechanism.^{15,17,46} We
 9 investigated the ORR process at a Pt(110) electrode surface in an alkaline solution similarly to the
 10 acid condition experiment (Fig. 4a, Supplementary Notes 9-10 and Supplementary Fig. 13-16).
 11 There was a broad Raman band around 1150 cm⁻¹ that appeared when the potential was decreased
 12 to 0.65 V. With a further decrease in the potential, this peak became stronger until 0.35 V and then
 13 decreased.



14

15 **Figure 4 | EC-SHINERS study of ORR at Pt(*hkl*) surfaces in alkaline condition.** EC-SHINERS spectra of

16 ORR at (a) Pt(110), (b) Pt(111) and (c) Pt(100) surfaces in 0.1 M NaClO₄ solution (pH~10.3) saturated with O₂.

17 The arrows represent the potential scanning direction, and all the potentials are relative to RHE.

18 To further investigate the effect of crystallographic orientation, comparative experiments were

1 conducted at other two low-index Pt(*hkl*) single crystal surfaces, Pt(111) and Pt(100), under same
2 identical condition (0.1 M NaClO₄ in H₂O with a pH~10.3). As Fig. 4b and 4c show, there was
3 almost a similar phenomenon in Fig. 4a, just with a little difference in starting potentials of the
4 peaks around 1150 cm⁻¹. This behavior indicated that there should with same intermediate species
5 at three low-index Pt(*hkl*) surfaces during ORR process in alkaline condition. A deuterium isotopic
6 substitution measurement was also carried out, and we found that the peaks around 1150 cm⁻¹ did
7 not exhibit obvious shift in alkaline condition (Supplementary Fig. 17-18). Thus, the intermediate
8 species around 1150 cm⁻¹ should be without “H”. Furthermore, the peak around 1150 cm⁻¹ was
9 obviously shifted to a lower wavenumber (around 1120 cm⁻¹) in 18-O₂ isotopic substitution
10 experiment at Pt(111) surface (Supplementary Note 11 and Supplementary Fig. 19), which
11 confirmed that the intermediates around 1150 cm⁻¹ could be attributed to oxygen related species.
12 In the previous studies, researchers had found that the characteristic Raman peak of superoxide
13 ion was around 1150 cm⁻¹ in the alkaline solution during the ORR process.¹⁵ Our DFT calculation
14 also proved that the peak around 1150 cm⁻¹ can be assigned to O-O stretching vibration of
15 superoxide ion O₂⁻ (Supplementary Tables 1-2, Supplementary Note 14 and Supplementary Fig.
16 24). In the calculation results, the adsorption of O₂⁻ with t-b site at Pt(110), Pt(100) and Pt(111),
17 and their Raman frequencies were located in 1162 cm⁻¹, 1177 cm⁻¹ and 1182 cm⁻¹, respectively,
18 which correlate very well with our experiment results. From the above information, we confirm
19 that the superoxide species has been identified as an important intermediate of ORR reaction at
20 Pt(*hkl*) surfaces in our research system.

21 A significant challenge for the ORR is that the reaction intermediates have a short lifetime and
22 thus are difficult to detect. Consequently, large concentrations of these intermediates are necessary

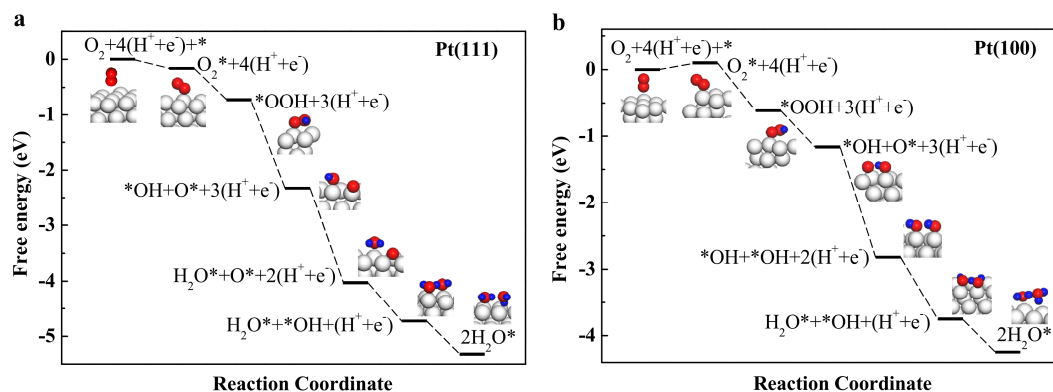
1 for their spectroscopic observation. Such conditions are not accomplished until sufficiently low
2 potentials are reached, when the reaction is fast enough to form large amounts of such
3 intermediates, commensurate with their rate of consumption. It is not unusual that this situation
4 should coincide with when the reaction starts to be diffusion-controlled, indicating that the
5 reaction is very fast and therefore the mass transport limits the reaction. However, it should be
6 mentioned that in the experiments reported in the present study, no obvious ORR intermediate
7 species are observed in the kinetic region. Evidently, more experimental evidences and theoretical
8 calculations to categorically show that the detailed ORR mechanism found in the
9 diffusion-controlled region maps directly onto the kinetic region will be required in future works.

10

11 **Mechanism of ORR process at Pt(*hkl*) surfaces**

12 Based on EC-SHINERS experiments and theoretical calculations, also include the consideration of
13 previous researches, the mechanism of ORR at the Pt(*hkl*) electrode surface in 0.1 M HClO₄
14 solution can be explained as follows: after adsorbing at the Pt(*hkl*) electrode surface, O₂⁻ formed
15 HO₂* via a proton and an electron transfer, which then quickly dissociated to form a pair of OH*
16 and O* on the neighboring Pt atoms. The OH* species further combined with “H” to generate H₂O.
17 The detailed schematic diagram of ORR mechanism at a Pt(*hkl*) surface as shown in Fig. 5a and
18 Fig. 5b (Supplementary Fig. 25). However, because of the different Gibbs free energy and
19 dissociation barrier of the same intermediates on different crystallographic planes, there are
20 differences between the Pt(111) and the other two facets (Pt(110) and Pt(100)) (Supplementary
21 Tables 3-6). (Based on the previous reports, the dissociation barriers for HO₂* on Pt(111) is about

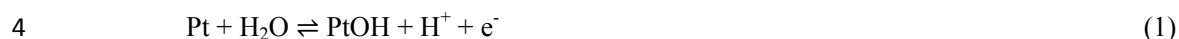
1 0.59 eV higher than that on Pt(100).⁴⁷⁻⁴⁹ During the ORR process, after protonation to form HO₂*
 2 at the Pt(111) surface, the adsorbed HO₂* species is stable and needs a higher activation energy to
 3 proceed to the next step (Fig. 5a). However, the instability of adsorbed HO₂* at Pt(110) and
 4 Pt(100) surfaces, coupled with simultaneously with a proton and an electron transfer process,
 5 leads to the O-O bond of HO₂* quickly breaking, and forming a pair of OH* and O* on the
 6 neighboring Pt atoms in acid condition (Fig. 5b). This should be correlated with the
 7 structure-activity relationship of different surfaces and the rate determining step of ORR. It is also
 8 in good agreement with previous references.^{9,10,47-50}



9
 10 **Figure 5 | The proposed mechanism of ORR at Pt(*hkl*) surfaces in 0.1 M HClO₄ solution and relevant Gibbs**
 11 **free energy (eV) of different intermediates at Pt(*hkl*) surfaces.** Free energies are given relative to gas-phase H₂
 12 and O₂ and metal surface to simulate the reaction of H₂+O₂→H₂O on Pt surface. Different intermediates at
 13 **a-Pt(111)** and **b-Pt(100)** surfaces. The white, red, and blue spheres represent Pt, O, and H, respectively. The
 14 mainly difference between **a** and **b** is the fourth step. For **a**, it is OH* + O* + 3(H⁺ + e⁻) → H₂O* + O* + 2(H⁺ + e⁻),
 15 while for **b**, it is OH* + O* + 3(H⁺ + e⁻) → OH* + OH* + 2(H⁺ + e⁻).
 16

17 Meanwhile, one idea that we have to have in mind is that, despite to the fact that adsorbed

1 species are detected or included in the calculations, solution species may exist and play a role. In
2 general the detected adsorption processes such as those shown in Equation 1 are fast and
3 reversible:



5 This may also happen with intermediates like HO_2^* which can go to the solution side,⁴⁰
6 interact strongly (H bonding) with the water layer and, eventually, become re-adsorbed before
7 further reaction. In this respect the ORR, once started, would involve intermediates that combine
8 hydrogen and oxygen atoms, which should be high mobility species in aqueous solution.

9

10 **Conclusions**

11 In this work, we employed *in situ* EC-SHINERS method to systematically investigate the ORR
12 process at $\text{Pt}(hkl)$ single crystal surfaces and obtained directly spectral evidences of OH^* , HO_2^*
13 and O_2^- . We found during the ORR process, the adsorbed HO_2^* is stable at the $\text{Pt}(111)$ surface, but
14 there is just adsorbed OH^* at the $\text{Pt}(110)$ and $\text{Pt}(100)$ surfaces. The steps to form HO_2^* and OH^*
15 species at the $\text{Pt}(hkl)$ surfaces will directly affect the ORR activity of different single crystal
16 surfaces. Meanwhile, in the alkaline condition, there were only O_2^- species found on three single
17 crystal surfaces. We therefore conclude that the protonation process significantly affects the ORR
18 activity and mechanism. Combining with the theoretical calculation results and previous
19 researches, we further explained the ORR mechanism at the $\text{Pt}(hkl)$ surface in acidic conditions,
20 and raised a reasonable interpretation and inference from EC-SHINERS measurements.

21

1 **Methods**

2 **Reagents.** Sodium citrate (99.0%), chloroauric acid (99.99%), sodium perchlorate (98.0% ~
3 102.0%), and (3-aminopropyl)trimethoxysilane(APTMS) (97%) were purchased from Alfa Aesar;
4 sodium hydroxide (97%, GR) and perchloric acid (70% ~ 72%, GR) were purchased from
5 Sinopharm chemical reagent Co. Ltd.; sodium silicate solution (27% SiO₂) was purchased from
6 Sigma-Aldrich. Deuterium oxide (for NMR 99.8 atom % D) was purchased from ARMAR AG. All
7 chemicals were used as received without further purification. Argon (99.999%), hydrogen
8 (99.999%) and oxygen (99.999%) were purchased from Linde gas. 18-O₂ (99.8%) was purchased
9 from LION Biology Company. Milli-Q water (~18.2 MΩ·cm) was used throughout the study.

10 **Equipments.** High-resolution TEM (JEOL, cat. no. JEM 2100 EX) and scanning electron
11 microscopy (SEM) (HITACHI S-4800) were used to characterize the morphology of SHINs and
12 single crystal surfaces. The electrode potential was controlled with an Autolab PGSTAT30
13 (Metrohm).

14 **Synthesis of SHINs.** We consider 55 nm Au@2 nm SiO₂ SHINs as an example to introduce the
15 detailed preparation process.²³ The 55 nm Au NPs were prepared according to Frens method First,
16 200 mL of 0.01% HAuCl₄ solution was taken into a 500 mL round-bottom flask and heated to
17 boiling under stirring. After that, 1.4 mL 1% sodium citrate solution was quickly added into the
18 above solution and continued the reaction for 40 min, and then cooled down at normal temperature
19 condition for the next step to prepare SHINs. SHINs were synthesized as following: 30 mL 55 nm
20 Au NPs solution was added into a round-bottom flask under stirring without heat, and then added
21 0.4 mL (3-Aminopropyl)trimethoxysilane (APTMS) (1 mM) were added. After 15 min reaction
22 under room temperature under stirring, 3.2 mL 0.54% Na₂SiO₃ solution (the pH was about 10.3)

1 were added into the above solution. After 3 min later, the mixed sample was transferred to a 98 °C
2 bath and stirred for 20 min. Then the solution was quickly cooled down in an ice-bath and
3 centrifuged for three times. Last, the concentrated SHINs was diluted with pure water for further
4 measurements.

5 **Electrochemistry.** The single crystal electrodes were Clavilier-type Pt(*hkl*) electrodes (the
6 diameter is ~2 mm). Before experiment, the Pt(*hkl*) electrodes were annealed in a butane flame and
7 cooled down in Ar + H₂ atmosphere. Electrochemical tests were conducted in a three-compartment
8 glass cell with a Pt wire as a counter electrode and an RHE reference electrode (all potentials are
9 reported with respect to RHE electrode in this paper). All solutions in the electrochemical ORR
10 measurements were saturated with oxygen. Electrochemical measurements were carried out with
11 an Autolab PGSTAT30 (Metrohm) and the ORR electrochemical experiments were researched at a
12 hanging meniscus rotating disk electrode (HMRDE) configuration system, using a Radiometer,
13 EDI-101. The pH value of 0.1 M NaClO₄ electrolyte was adjusted by NaOH solution.

14 **The cleaning process for the SHINs on Pt(*hkl*) surfaces.** Place the Pt(*hkl*) electrode (modified
15 with SHINs) in an electrochemical cell filled with 0.1 M NaClO₄ solution (pH~9), and polarize at
16 -1.2 V (vs. SCE) for about 1-2 min (the generation of tiny hydrogen gas could be observed). The
17 HER proceeded vigorously, and the impurities adsorbed on the electrode or SHINs surface would
18 be desorbed and diffused into the solution. Wash the electrode surface carefully and change the
19 solution. Repeat these processes 3-5 times. Finally, transfer the electrode to another clean
20 electrochemical cell or Raman cell for CV or *in situ* Raman tests.

21 ***In situ* EC-SHINERS.** Raman spectra were recorded with an Xplora confocal microprobe Raman
22 system (HORIBA JobinYvon). A 50× magnification long working distance (8 mm) objective was

1 used. The wavelength of excitation laser was 637.8 nm from a He-Ne laser (power was about 6
2 mW). Raman frequencies were calibrated using Si wafer and ClO_4^- solution spectra. The Raman
3 spectra shown in the experiment were collected during 120 s for one single spectrum curve one
4 time, accumulation twice.

5 **3D-FDTD numerical method.** The 3 dimensional finite-difference time-domain (3D-FDTD)
6 method was used to study the electromagnetic field enhancement. The fundamental principle of
7 FDTD can refer to the literature.³³ The FDTD has been widely used to investigate the optical
8 properties, such as light scattering, absorption and electromagnetic field distributions. In the
9 simulation, perfectly matched layer (PML) was used. The simulation time was set as 1000 fs that
10 was enough to insure the convergence of calculation. We adapted non-uniform mesh size in the
11 junctions of the investigated structures. In detail, the Yee cell size in the junctions of
12 particle-particle and particle-Pt film is $0.25 \text{ nm} \times 0.25 \text{ nm} \times 0.25 \text{ nm}$ and the remaining regions
13 was $0.5 \text{ nm} \times 0.5 \text{ nm} \times 0.5 \text{ nm}$. The dielectric function of Pt and Au that were dependent on
14 wavelength were taken from a multi-coefficient fitting model offered by Lumerical FDTD.

15 **Computational details.** All theoretical simulations were performed using the
16 Perdew-Burke-Ernzerhof (PBE) functional of generalized gradient approximation (GGA)⁵¹ to
17 simulate Periodic boundary condition (PBC) model implemented in the Vienna ab initio
18 simulation package (VASP)⁵². The projector-augmented wave (PAW) method was applied to
19 describe the electron-ion interactions. A plane-wave basis cutoff of 400 eV was used for the wave
20 functions, energies were converged to 10^{-5} eV. Paxton and Methfessel method with a broadening
21 factor of 0.1 eV was used, and the Γ -centered k -point sampling grid of $12 \times 12 \times 12$ was applied for
22 the primitive cell calculation was adopted. The Γ -centered k -point sampling grid of $6 \times 6 \times 1$ was

1 adopted for all single crystal facets concerned in this work. Vibrational frequencies of adsorbed
2 molecules on surface metal were calculated with density-functional perturbation theory (DFPT).
3 The bottom 2 layers of the five-layer 2×2 Pt surface are fixed, while the top 3 layers are relaxed in
4 all calculation. In addition, spin-polarized calculation was performed in the geometry optimization.
5 For the DFT calculation of O₂⁻, the electron in our system is simulated by adding one electron,
6 while the charge neutrality is maintained by a compensating uniform charge background.⁵³ The
7 calculated lattice constant of Pt was 3.977 Å, which agrees with the experimental value of 3.909 Å,
8 and the vacuum spaces of 15 Å was used to describe the five layers 2 × 2 Pt surface. All
9 thermodynamic energies were calculated at 298.15 K and 1atm using the Atomic Simulation
10 Environment suite of programs (Equation 2).⁵⁴

$$11 \quad G = H - TS = E_{DFT} + E_{ZPE} + \int_0^{298.15K} C_v dT - TS \quad (2)$$

12 Where E_{DFT} is the total energy from DFT geometry optimization, E_{ZPE} is the zero-point vibrational
13 energy (ZPE), $\int_0^{298.15K} C_v dT$ the thermal energy is heat capacity, T is the temperature, and the S
14 is entropy. The ideal gas approximation was used for O₂ and H₂, and the harmonic approximation
15 was used for adsorbates.

16 **Data availability.** The data that support the plots within this paper and other findings of this study
17 are available from the corresponding author upon reasonable request.

18

19 **References**

- 20 1. Stamenkovic, V. R., Strmcnik, D., Lopes, P. P. & Marković, N. M. Energy and fuels from
21 electrochemical interfaces. *Nat. Mater.* **16**, 57-69 (2016).
- 22 2. Conder, J. *et al.* Direct observation of lithium polysulfides in lithium-sulfur batteries using

- 1 *operando* X-ray diffraction. *Nat. Energy* **2**, 17069 (2017).
- 2 3. Perry, R. H., Cahill III, T. J., Roizen, J. L., Bois, J. D. & Zare, R. N. Capturing fleeting
3 intermediates in a catalytic C-H amination reaction cycle. *Proc. Natl. Acad. Sci. U. S. A.* **109**,
4 18295-18299 (2012).
- 5 4. Li, J. *et al.* Surface evolution of a Pt-Pd-Au electrocatalyst for stable oxygen reduction. *Nat.*
6 *Energy* **2**, 17111 (2017).
- 7 5. Greeley, J. *et al.* Alloys of platinum and early transition metals as oxygen reduction
8 electrocatalysts. *Nat. Chem.* **1**, 552-556 (2009).
- 9 6. Xia, B. Y. *et al.* A metal-organic framework-derived bifunctional oxygen electrocatalyst. *Nat.*
10 *Energy* **1**, 15006 (2017).
- 11 7. Bu, L. Z. *et al.* Biaxially strained PtPb/Pt core/shell nanoplate boosts oxygen reduction
12 catalysis. *Science* **354**, 1410-1414 (2016).
- 13 8. Postlethwaite, T. A., Hutchison, J. E., Murray, R., Fosset, B. & Amatore, C. Interdigitated array
14 electrode as an alternative to the rotated ring-disk electrode for determination of the reaction
15 products of dioxygen reduction. *Anal. Chem.* **68**, 2951-2958 (1996).
- 16 9. Gómez-Marín, A. M., Rizo, R. & Feliu, J. M. Oxygen reduction reaction at Pt single crystals: A
17 critical overview. *Catal. Sci. Technol.* **4**, 1685-1698 (2014).
- 18 10. Nørskov, J. K. *et al.* Origin of the overpotential for oxygen reduction at a fuel-cell cathode. *J.*
19 *Phys. Chem. B* **108**, 17886-17892 (2004).
- 20 11. Strmcnik, D. *et al.* The role of non-covalent interactions in electrocatalytic fuel-cell reactions
21 on platinum. *Nat. Chem.* **1**, 466-472 (2009).
- 22 12. Ledezma-Yanez, I. *et al.* Interfacial water reorganization as a pH-dependent descriptor of the

- 1 hydrogen evolution rate on platinum electrodes. *Nat. Energy* **2**, 17031 (2017).
- 2 13. Kunimatsu, K., Yoda, T., Tryk, D. A., Uchida, H. & Watanabe, M. *In situ* ATR-FTIR study of
3 oxygen reduction at the Pt/Nafion interface. *Phys. Chem. Chem. Phys.* **12**, 621-629 (2010).
- 4 14. Gewirth, A. A., Li, X. Oxygen electroreduction through a superoxide intermediate on
5 Bi-modified Au surfaces. *J. Am. Chem. Soc.* **127**, 5252-5260 (2005).
- 6 15. Gewirth, A. A. & Kim, J. Mechanism of oxygen electroreduction on gold surfaces in basic
7 media. *J. Phys. Chem. B* **110**, 2565-2571 (2006).
- 8 16. Itoh, T., Maeda, T. & Kasuya, A. *In situ* surface-enhanced Raman scattering
9 spectroelectrochemistry of oxygen species. *Faraday Discuss.* **132**, 95-109 (2006).
- 10 17. Shao, M. H., Liu, P. & Adzic, R. R. Superoxide anion is the intermediate in the oxygen
11 reduction reaction on platinum electrodes. *J. Am. Chem. Soc.* **128**, 7408-7409 (2006).
- 12 18. Johnson, L. *et al.* The role of LiO₂ solubility in O₂ reduction in aprotic solvents and its
13 consequences for Li-O₂ batteries. *Nat. Chem.* **6**, 1091-1099 (2014).
- 14 19. Ohta, N., Nomura, K. & Yagi, I. Adsorption and electroreduction of oxygen on gold in acidic
15 media: *In situ* spectroscopic identification of adsorbed molecular oxygen and hydrogen
16 superoxide. *J. Phys. Chem. C* **116**, 14390-14400 (2012).
- 17 20. Fleischmann, M., Hendra, P. J. & McQuillan, A. J. Raman spectra of pyridine adsorbed at a
18 silver electrode. *Chem. Phys. Lett.* **26**, 163-166 (1974).
- 19 21. Jeanmaire, D. L. & Van Duyne, R. P. Surface Raman spectroelectrochemistry: Part I.
20 Heterocyclic, aromatic, and aliphatic-amines adsorbed on anodized silver electrode. *J.*
21 *Electroanal. Chem.* **84**, 1-20 (1977).
- 22 22. Moskovits, M. Surface-enhanced spectroscopy. *Rev. Mod. Phys.* **57**, 783-826 (1985).

- 1 23. Li, J. F. *et al.* Shell-isolated nanoparticle-enhanced Raman spectroscopy. *Nature* **464**, 392-395
2 (2010).
- 3 24. Li, J. F. *et al.* Extraordinary enhancement of Raman scattering from pyridine on single crystal
4 Au and Pt electrodes by shell-isolated Au nanoparticles. *J. Am. Chem. Soc.* **133**, 15922-15925
5 (2011).
- 6 25. Ding, S. Y. *et al.* Nanostructure-based plasmon-enhanced Raman spectroscopy for surface
7 analysis of materials. *Nat. Rev. Mater.* **1**, 16021-16036 (2016).
- 8 26. Butcher, D. P., Boulos, S. P., Murphy, C. J., Ambrosio, R. C. & Gewirth, A. A. Face-dependent
9 shell-isolated nanoparticle enhanced Raman spectroscopy of 2,2'-bipyridine on Au(100) and
10 Au(111). *J. Phys. Chem. C* **116**, 5128-5140 (2012).
- 11 27. Honesty, N. R. & Gewirth, A. A. Shell-isolated nanoparticle enhanced Raman spectroscopy
12 (SHINERS) investigation of benzotriazole film formation on Cu(100), Cu(111), and Cu(poly).
13 *J. Raman Spectrosc.* **43**, 46-50 (2012).
- 14 28. Li, J. F., Rudnev, A., Fu, Y., Bodappa, N. & Wandlowski, T. *In situ* SHINERS at
15 electrochemical single-crystal electrode/electrolyte interfaces: Tuning preparation strategies
16 and selected applications. *ACS Nano* **7**, 8940-8952 (2013).
- 17 29. Guan, S. L. *et al.* Structure sensitivity in catalytic hydrogenation at platinum surfaces measured
18 by shell-isolated nanoparticle enhanced Raman spectroscopy (SHINERS). *ACS Catal.* **6**,
19 1822-1832 (2016)
- 20 30. Li, C. Y. *et al.* *In situ* monitoring of electrooxidation processes at gold single crystal surfaces
21 using shell-isolated nanoparticle-enhanced Raman spectroscopy. *J. Am. Chem. Soc.* **137**,
22 7648-7651 (2015).

- 1 31. Li, J. F. *et al.* Electrochemical shell-isolated nanoparticle-enhanced Raman spectroscopy:
2 Correlating structural information and adsorption processes of pyridine at the Au(*hkl*) single
3 crystal/solution interface. *J. Am. Chem. Soc.* **137**, 2400-2408 (2015).
- 4 32. Galloway, T. A. & Hardwick, L. J. Utilizing *in situ* electrochemical SHINERS for oxygen
5 reduction reaction studies in aprotic electrolytes. *J. Phys. Chem. Lett.* **7(11)**, 2119-2124 (2016).
- 6 33. Taflove, A. & Hagness, S. C. *Computational Electrodynamics: the Finite-Difference*
7 *Time-Domain Method* (Artech House Press, 2005).
- 8 34. Yee, K. S. Numerical solution of initial boundary value problems involving Maxwell's
9 equations in isotropic media. *IEEE Trans. Antennas Propag.* **14**, 302-307 (1966).
- 10 35. Chen, S. *et al.* How to light special hot spots in multiparticle-film configurations. *ACS Nano* **10**,
11 581-587 (2016).
- 12 36. Chen, S. *et al.* Electromagnetic enhancement in shell-isolated nanoparticle-enhanced Raman
13 scattering from gold flat surfaces. *J. Phys. Chem. C* **119**, 5246-5251 (2015).
- 14 37. Marković, N. M, Gasteiger, H. & Ross, P. N. Kinetics of oxygen reduction on Pt(*hkl*)
15 electrodes: Implications for the crystallite size effect with supported Pt electrocatalysts. *J.*
16 *Electrochem. Soc.* **144**, 1591-1597 (1997).
- 17 38. Kuzume A., Herrero E. & Feliu J. M. Oxygen reduction on stepped platinum surfaces in acidic
18 media. *J. Electroanal. Chem.* **599**, 333-343 (2007).
- 19 39. Gomez-Marin, A. M. & Feliu, J. M. New insights into the oxygen reduction reaction
20 mechanism on Pt(111): A detailed electrochemical study. *ChemSusChem* **6**, 1091-1100 (2013).
- 21 40. Briega-Martos, V., Herrero, E., & Feliu, J. M. Effect of pH and water structure on the oxygen
22 reduction reaction on platinum electrodes. *Electrochim. Acta* **241**, 497-509 (2017).

- 1 41. Zhang, Y. & Weaver, M. J. Application of surface-enhanced Raman-spectroscopy to organic
2 electrocatalytic systems: Decomposition and electrooxidation of methanol and formic-acid on
3 gold and platinum-film electrodes. *Langmuir* **9**, 1397-1403 (1993).
- 4 42. Climent, V., Gomez, R., Orts, J. M. & Feliu, J. M. Thermodynamic analysis of the temperature
5 dependence of OH adsorption on Pt(111) and Pt(100) electrodes in acidic media in the absence
6 of specific anion adsorption. *J. Phys. Chem. B* **110**, 11344-11351(2006).
- 7 43. Gómez-Marín, A. M., Clavilier, J. & Feliu, J. M. Sequential Pt(111) oxide formation in
8 perchloric acid: An electrochemical study of surface species inter-conversion. *J. Electroanal.*
9 *Chem.* **688**, 360-370 (2013).
- 10 44. Zhao, M. & Anderson, A. B. Predicting the double layer width on Pt(111) in acid and base
11 with theory and extracting it from experimental voltammograms. *J. Phys. Chem. C* **121**,
12 28051-28064 (2017).
- 13 45. Tanaka, H. *et al.* Infrared reflection absorption spectroscopy of OH adsorption on the low
14 index planes of Pt. *Electrocatalysis* **6**, 295-299 (2014).
- 15 46. Briega-Martos, V. *et al.* An aza-fused π -conjugated microporous framework catalyzes the
16 production of hydrogen peroxide. *ACS Catal.* **7**, 1015-1024 (2016).
- 17 47. Keith, J. A. & Jacob, T. Theoretical studies of potential-dependent and competing mechanisms
18 of the electrocatalytic oxygen reduction reaction on Pt(111). *Angew. Chem. Int. Ed.* **49**,
19 9521-9525 (2010).
- 20 48. Keith, J. A., Jerkiewicz, G. & Jacob, T. Theoretical investigations of the oxygen reduction
21 reaction on Pt(111). *ChemPhyschem* **11**, 2779-2794 (2010).
- 22 49. Duan, Z. & Wang, G. Comparison of reaction energetics for oxygen reduction reactions on

1 Pt(100), Pt(111), Pt/Ni(100), and Pt/Ni(111) surfaces: A first-principles study. *J. Phys. Chem.*
2 *C* **117**, 6284-6292 (2013).

3 50. Tian, F. & Anderson, A. B. Effective reversible potential, energy loss, and overpotential on
4 platinum fuel cell cathodes. *J. Phys. Chem. C* **115**, 4076-4088 (2011).

5 51. Perdew, J. P., Burke, K. & Ernzerhof, M. Generalized gradient approximation made simple.
6 *Phys. Rev. Lett.* **77**, 3865-3868 (1996).

7 52. Kresse, G. & Furthmuller, J. Efficient iterative schemes for ab initio total-energy calculations
8 using a plane-wave basis set. *Phys. Rev. B* **54**, 11169-11186 (1996).

9 53. Makov, G. & Payne, M. C. Periodic boundary conditions in *ab initio* calculations. *Phys. Rev. B*
10 **51**, 4014-4022 (1995).

11 54. Bahn, S. R. & Jacobsen, K. W. An object-oriented scripting interface to a legacy electronic
12 structure code. *Comput. Sci. Eng.* **4**, 56-66 (2002).

13

14 **Acknowledgements**

15 This work was supported by the NSFC (21522508, 21427813, 21521004, 21533006, 21621091,
16 and 21775127), "111" Project (B16029 and B17027), Natural Science Foundation of Guangdong
17 Province (2016A030308012), the Fundamental Research Funds for the Central Universities
18 (20720180037), and the Thousand Youth Talents Plan of China. Support from MINECO and
19 Generalitat Valenciana (Spain), through projects CTQ2016-76221-P (AEI/FEDER, UE) and
20 PROMETEOII/2014/013 respectively, is greatly acknowledged. V.B.M thankfully acknowledges
21 to MINECO the award of a pre-doctoral grant (BES-2014-068176, project CTQ2013-44803-P).

1 We thank H. Zhang, M. Su, Y. H. Wang, J. Cheng, G. Attard, B. Ren, Z.Y. Zou, B.A. Lu, and X.D.
2 Yang for discussions.

3

4 **Author Contributions**

5 J.C.D., V.B.M., and J.Y. carried out the experiments. X.G.Z., J.X., and D.Y.W. conducted the DFT
6 calculations. S.C. and Z.L.Y. conducted the FDTD simulations. J.M.F, C.T.W, J.F.L., and Z.Q.T.
7 designed the experiments. All authors contributed to the preparation of the manuscript.

8

9 **Supplementary Information**

10 Supplementary Notes 1-14, TEM, DFT calculations, Supplementary Figures 1-25 and
11 Supplementary Tables 1-6 are provided in the Supplementary Information. This information is
12 available free of charge via the Internet.

13

14 **Competing interests**

15 The authors declare no competing interests.